Capillary electrophoresis with dual detection UV/C4D for monitoring myrosinase-mediated hydrolysis of thiol glucosinolate designed for gold nanoparticle conjugation

Bérengère Claude, Giuliano Cutolo, Amal Farhat, Irina Zarafu, Petre Ionita, Marie Schuler, Arnaud Tatibouët, Philippe Morin, Reine Nehmé

Capillary electrophoresis with dual detection UV/C^{4}D for monitoring myrosinase-mediated hydrolysis of thiol glucosinolate designed for gold nanoparticle conjugation

Bérengère Claude[£], Giuliano Cutolo[£], Amal Farhat[£], Irina Zarafu[¤], Petre Ionita[¤], Marie Schuler[£], Arnaud Tatibouët[£], Philippe Morin[£], Reine Nehmé[£]*

[£] Institut de Chimie Organique et Analytique (ICOA), Université d'Orléans - CNRS FR 2708 - UMR 7311, Orléans, France

[¤] University of Bucharest, Faculty of Chemistry, Organic Chemistry, Biochemistry and Catalysis Department, Soseaua Panduri 90-92, Sect. 5, Bucharest, Romania

* Corresponding author: Dr. Reine Nehmé, Institut de Chimie Organique et Analytique (ICOA), Université d'Orléans, BP 6759, rue de Chartres, 45067 Orléans cedex 2, France.
e-mail: reine.nehme@univ-orleans.fr ; Tel: +33-2-38-49-27-75 ; Fax: +33-2-38-41-72-81

List of abbreviations: **AuNPs**, gold nanoparticles; **C^{4}D**, contactless capacitively coupled conductivity detector; **CPA,** corrected peak area; **GLs**, glucosinolates; **GL-SH**, thiol glucosinolate; **ITCs**, isothiocyanates; **K_m**, Michaelis–Menten constant; **NPs**, nanoparticles; **TDLFP**, transverse diffusion of laminar flow profiles; **V_{max}**, maximum velocity.

Keywords: capillary electrophoresis, conjugation, contactless conductivity detector, enzyme assay, gold nanoparticles

Abstract

Capillary electrophoresis (CE) with dual UV and conductivity detection was used for the first time to monitor the functionalization of gold nanoparticles (AuNPs), a process catalyzed by an enzyme, myrosinase (Myr). A thiol glucosinolate (GL-SH) designed by our group was used as substrate.

Hydrolysis of free and immobilized GL-SH was characterized using off-line and on-line CE-based enzymatic assays. The developed approaches were validated using sinigrin, a well-referenced substrate of Myr. Michaelis-Menten constant of the synthetized GL-SH was comparable to sinigrin, showing that they both have similar affinity towards Myr. It was demonstrated that transverse diffusion of laminar flow profiles was well adapted for in-capillary Mixing of nanoparticles (AuNPs) with proteins (Myr) provided that the incubation time is inferior to 20 min. Only low reaction volume (nL to few µL) and short analysis time (< 5 min) were required. The electrophoretic conditions were optimized in order to evaluate and to confirm the AuNPs stability before and after functionalization by CE/UV based on surface plasmon resonance band red-shifting. The hydrolysis of the functionalized AuNPs was subsequently evaluated using the developed CE-C^4D/UV approach. Repeatabilities of enzymatic assays, of electrophoretic analyses and of batch-to-batch functionalized AuNPs were excellent.

1. Introduction

Capillary electrophoresis (CE) is a cost-effective and a powerful tool for enzyme, substrate and inhibitor screening and characterization [1-5]. There are two main approaches for studying enzymes by CE. In off-line or pre-capillary assays [6], the enzymatic reaction takes place in a vial outside the capillary and a few nanoliters of the reaction mixture are injected into the capillary. The product formed is then separated from excess reagents, detected and quantified. In on-line assays [7-9], the enzymatic reaction takes place directly in the CE capillary that acts as an enzymatic nanoreactor. The small volume requirement enables analysis of reactants in very limited supply [7-11]. Kinetic and affinity constants (Michaelis-Menten or inhibition determinations; V_{max} and K_m, IC_{50}) ranging from nM to mM can be determined [1-3,7-11]. Enzymes can also be used tethered to a monolithic support or to particles in order to improve their stability and reusability [12,13]. The compatibility of CE with various detectors *e.g.* UV-visible absorption, laser induced fluorescence (LIF), contactless capacitively coupled conductivity detector (C^4D) [14,15] and mass spectrometry (MS) makes it suitable for various enzymatic systems. Structural information is obtained by CE-MS, for example after in-line digestion of peptides and proteins [16-21]. CE-C^4D allows the quantification of small inorganic ions even at ppt levels [22,23].

On the other hand, CE is useful for investigating the quality and the stability (aggregation) of nanoparticles (NP) functionalized with a variety of molecules [24-27]. NP (1-100 nm) exhibit unique chemical and physical properties depending on their chemical composition, shape, size, surface, and local environment [28-32]. Gold nanoparticles (AuNPs) are one of the most studied nano-objects. Physicochemical characterization of AuNPs is mainly performed using light scattering [33], electron or atomic force microscopies, atomic spectroscopy, and electroanalytical techniques [34,35]. Separation methods are also used such as size exclusion chromatography, flow field fractionation as well as gel and capillary electrophoresis [24-27,36]. The surface of AuNPs has been continuously modified through binding of functional groups or molecules to provide stability, selectivity and functionality for various applications

[37,38]. AuNPs have been reported in separation sciences [26,39], electronics, optical and electronic devices, catalytic applications, and in bio-nanotechnology (diagnosis, imaging and drug delivery) because of their excellent biocompatibility and low toxicity [28-31,35-38,40]. For example, the *in-vitro* anticancer effect of broccoli phytochemicals, mainly glucosinolates (GLs), isothiocyanates (ITCs) and flavonoids, was enhanced when conjugated to AuNPs as a drug delivery system [41]. Moreover, extracts of watercress and of *Brassica oleracea L.* [42], containing high quantities of GLs, were used to biosynthesize AuNPs with biocide properties.

In this work, CE was employed as a technique of choice to monitor an original conjugation strategy for AuNPs that we introduce. For this, a glucosinolate bearing a terminal thiol moiety (GL-SH) was designed and synthetized (Figure 1). The hydrolysis of this GL-SH by the myrosinase (Myr), a thioglucoside glucohydrolase, will allow capping the AuNP surface with an ITC precursor (Schema 1) [43]. This latter can be used as a bio-conjugation tool allowing efficient threading of molecules of interest onto AuNP. Indeed, the myrosinase-glucosinolate reaction, a unique biochemical transformation in the nature [44], produces highly reactive ITCs that can further react with nucleophiles for *in vitro* chemical ligation [45,46]. To our knowledge no glucosinolate capped AuNP has neither been developed, nor studied using CE.

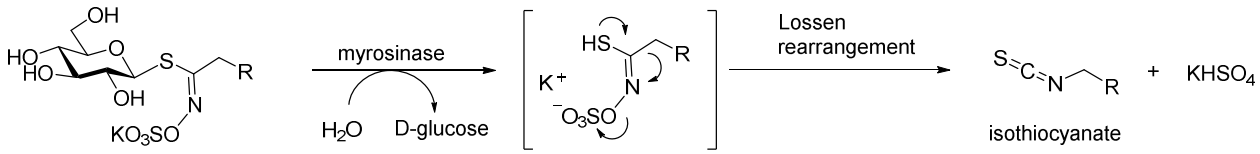

Schema 1: Myrosinase-mediated hydrolysis of a glucosinolate into isothiocyanate and sulfate

Before conducting enzymatic reaction, CE analyses were optimized to simultaneously detect GL-SH by UV absorption and sulfate by C^4D. This allows a simultaneous follow-up of both the decrease of the substrate GL-SH and the increase of the sulfate as the by-product of the catalyzed reaction. To monitor the hydrolysis by Myr of free and immobilized GL-SH on AuNPs, CE with dual detection UV/C^4D was used. Our previous off-line CE-C^4D assay [47] was optimized and adapted for this study. For economy features, an on-line Myr assay based on transverse diffusion of laminar flow profiles (TDLFP) [48,49] was developed. The linearity

of the Myr action on the synthetized GL-SH was assessed. For validation purposes, we analyzed the sinigrin, a well-referenced substrate of Myr, using both the off-line and the novel on-line approaches. Citrate-capped AuNPs were chosen since they are the most frequently used particles, as they often represent a first step of synthesis before being grafted [25]. Their stability was also monitored using CE based on the approach proposed by Haes et al. [24] since a significant red-shifting of the surface plasmon resonance band is induced by aggregation [24,38]. Repeatability of enzymatic assays, of electrophoretic analyses and of batch-to-batch functionalized AuNPs were evaluated in order to confirm the reliability of the developed CE methods.

2. Materials and methods

2.1 Chemicals

AuNP (20 nm o.d., stabilized suspension at 1.09 nM in citrate buffer), citric acid ($C_6H_8O_7$, purity ≥ 99.5%), 3-(Cyclohexylamino)-1-propanesulfonic acid (CAPS, $C_6H_{11}NH(CH_2)_3SO_3H$, purity ≥ 98 %), glacial acetic acid (AcOH, CH_3CO_2H, purity ≥ 99.99 %), L-histidine ($C_6H_9N_3O_2$, purity ≥ 99.5 %), orthophosphoric acid (H_3PO_4, 85 % w/w in water), potassium phosphate dibasic trihydrate (K_2HPO_4, $3H_2O$, purity ≥ 99.0 %), potassium phosphate monobasic (KH_2PO_4, purity ≥ 99.0 %), sodium dodecyl sulfate (SDS, $C_{12}H_{25}NaO_4S$, purity ≥ 98.5 %), sodium hydroxide (NaOH, purity ≥ 98 %), sodium sulfate (Na_2SO_4, purity ≥ 99.0 %), sodium tetraborate ($Na_2B_4O_7$, purity ≥ 99 %), (−)sinigrin hydrate ($C_{10}H_{16}NO_9S_2{\cdot}K{,}{\cdot}xH_2O$, purity 99.0 %) and thioglucosidase from *Sinapis alba* (myrosinase (Myr), EC 3.2.1.147, 25 U, ≥100 units.g^{-1}) were purchased from Sigma-Aldrich (Saint-Quentin Fallavier, France). Bidistilled 18 MΩ cm water was from Carlo Erba (Val de Reuil, France). All chemicals were used as received. All product bottles were placed in tightly closed plastic bags to preserve them from aerosol contaminations [50] and then stored at 4°C.

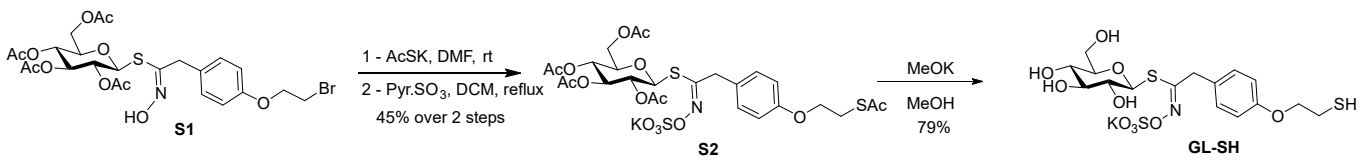

Schema 2: Thiol glucosinolate (GL-SH) synthesis

Thiol glucosinolate (GL-SH) was synthesized using methodologies developed within our group from known bromoglucosinolate **S1** (schema 2, [46]). Nucleophilic substitution with potassium thioacetate, followed by sulfatation using pyridinium sulfur trioxyde led to the corresponding acetylated thioglucosinolate **S2** which was then deacetylated using modified Zemplen conditions to deliver the desired **GL-SH** in good yield (79 %).

2.2 Equipment and operating conditions

Experiments were carried out on an HP^3D capillary electrophoresis system (Agilent, Waldbronn, Germany). Agilent software 3D-CE Chemstation (rev B.04.02) was used to pilot the CE. This instrument was equipped with an on-capillary TraceDec C^4D detector (Innovative Sensor Technologies GmbH, Strasshof, Austria) and a UV-Vis diode-array detector. The following parameters were fixed for the C^4D: frequency medium; voltage 0 dB; gain 100 %; offset 130; filter: frequency 1/3 and cut-off 0.05. The C^4D detection signal was acquired with the Tracemon software (Istech, version 0.07a).

Unless otherwise stated, CE analyses were conducted in an uncoated silica capillary of 31 cm total length and 50 µm i.d. (Polymicro Technologies, Phoenix, AZ, USA). The effective detection length was 8.5 cm to the UV detection and 19 cm to the C^4D (short-end injection). New capillaries were conditioned by performing the following rinses: 1 M LiOH (15 min), water (5 min) and background electrolyte or BGE (10 min). Between runs, the capillary was rinsed with the BGE for 3 min. Rinse cycles were conducted at 950 mbar. At the end of each working-day, the capillary was rinsed for 10 min with water before storing it overnight.

Polypropylene flasks, containers, CE vials and polyethylene olefin snap caps were used since they have little extractable material unlike glass. To avoid inadvertent contamination, nitrile – powder free – gloves were worn during solution preparation. To ensure good-quality cleaning, all volumetric equipment, vials and snap caps were rinsed with water (18 MΩ cm), and then soaked in water for an overnight period.

2.3 Solutions

All solutions were prepared with ultra-pure bidistilled water, filtered through a 0.45 µm polyvinylidenedifluoride (PVDF) Millex-HV Syringe Filter (Millipore, Molsheim, France) before use and stored at 4° C when not in use. Phosphate buffer (KH_2PO_4/K_2HPO_4) was used as an incubation buffer (IB) at an ionic strength (I) of 33 mM. Its pH was adjusted to 7.0 by addition of 1 M NaOH. For electrophoretic separation, each tested BGE was degassed by ultra-sonication before use. The BGE solution in the separation vials was changed every three runs. BGE parameters were given by Phoebus software (Analis, Namur, Belgium). The pH was measured with a MeterLab PHM201 pH-Meter (Radiometer Analytical, Villeurbanne, France).

Stock solutions of each glucosinolate substrate (100 mM), Na_2SO_4 (100 mM) and Myr (0.5 $U.mL^{-1}$) were prepared by dissolving the appropriate quantity of each compound – accurately weighed – in the IB. Working solutions were prepared by appropriate dilution of the corresponding stock solution in the IB. Substrates must be used at large excess compared to enzyme (about 100 times). For this, Myr was used at 0.05 $U.mL^{-1}$ for all enzymatic assays.

The response function of the C^4D detector was examined by plotting the corrected-peak areas (CPA) *versus* SO_4^{2-} concentrations. The calibration curve was performed over the concentration range 0.015–15 mM sulfate. Three independent determinations were performed at each concentration. Repeatability was expressed as relative standard deviation (RSD) on the migration times and on the CPA.

For the functionalization of nanoparticles, 40 µL of aqueous solution of GL-SH (10 mM) was added to 210 µL of AuNP citrates and the solution kept at ambient temperature for 18 h. Then, the solution was centrifuged at 10000 rpm during 30 min at 10 °C in order to settle the functionalized gold nanoparticles (NP-GL) and discard the supernatant containing unbounded GL-SH. The residue of NP-GL was suspended in 250 µL of water and centrifuged again. The whole process was repeated twice. The cleaned NP-GL were suspended in 210 µL-volume of IB. Figure 1 shows the mechanism of the AuNP functionalization.

158 **2.4 Evaluation of gold nanoparticles stability by CE-UV**

159 To evaluate gold nanoparticle stability, a silica capillary of 40 cm total length (31.5 cm effective length and
160 50 µm i.d) was used. 10 µL of NP citrates or NP-GL were placed in a micro-vial of the CE instrument auto-
161 sampler at room temperature. The sample was then injected into the capillary at the anode (normal-end
162 injection) by applying a positive pressure of 50 mbar for 30 s (injected volume 57 nL). The BGE was 10 mM
163 CAPS-70 mM SDS buffer (pH 10) and the electrophoretic separation was performed at 25 °C under + 20 kV
164 (current of 61 µA).

165 The stability of AuNPs was then estimated by calculating the ratio (R) of the absorbance at 520 nm over the
166 absorbance at 600 nm (equation 1) [24]:

167 $$R=\frac{\text{absorbance (520)}}{\text{absorbance (600)}} \qquad (1)$$

168 **2.5 Enzymatic study**

169 ***- Pre-capillary assays:*** This pre-capillary assay is based on the one we developed earlier in our laboratory
170 [47]. Unless otherwise stated, enzymatic reaction was conducted at 37±1 °C. The reaction mixture (11 µL)
171 contained 1 µL of the Myr (0.05 $U.mL^{-1}$) and 10 µL of the substrate solution dissolved in the incubation
172 phosphate buffer (pH 7.0). It was poured in a micro-vial of the CE instrument auto-sampler.

173 The linearity of the Myr activity toward the thiol GL, free or immobilized on AuNPs, was evaluated by
174 monitoring simultaneously the increase over the time of the product SO_4^{2-} by the C^4D and the decrease of the
175 substrate GL-SH by UV detection at 230 nm (due to the presence of the aromatic ring chromophore). For
176 this, the enzymatic reaction was conducted with GL-SH at 1.6 mM and the incubation time was varied using
177 a time interval of 10 min.

178 To estimate K_m and V_{max} values, the incubation time was 10 min so that the substrate conversion does not
179 exceed 10 %. The stock solution of each tested glucosinolate was diluted to obtain a range of concentrations,
180 from 0.01 to 3 mM for GL-SH and 0.01 to 2.5 mM for sinigrin.

Before CE analyses, the enzymatic reaction was stopped by heating the mixture with an oil bath at 130 °C±5 °C for 5 min. The reaction mixture was then injected into the capillary at the cathode (short-end injection) by applying a negative pressure of -50 mbar for 10 s (24.6 nL). Unless otherwise stated, the electrophoretic separation was performed at 25 °C under +20 kV in the His-AcOH buffer (current of 30 µA). Blank assays were conducted according to the same procedure without adding the Myr or the substrate.

The solutions used to assess the calibration curve for SO_4^{2-} underwent the same treatments in order to avoid any error due to evaporation in the oil bath. The reaction rate V_i ($mM.min^{-1}$) was calculated as the ratio of the concentration of SO_4^{2-} formed *per* time interval.

- On-line assays: The TDLFP approach was used for in-capillary mixing of Myr with the GL. After filling the capillary with the BGE, the reagents were introduced as follows: IB (-25 mbar for 10 s; ~12.3 nL), Myr (-50 mbar for 5 s; ~12.3 nL), GL (-50 mbar for 5 s; ~12.3 nL) and IB (-50 mbar for 10 s; ~24.6 nL). The concentrations of the reactants in the solutions used for on-line assays were twice the concentration used for pre-capillary assays; 0.1 $U.mL^{-1}$ for Myr, 0.02 to 6 mM for GL-SH and 0.02 to 5 mM for sinigrin. After in-capillary mixing, the concentration of each reactant is expected to be divided by two since two plugs of reactants were introduced in the capillary.

For on-line assays of the hydrolysis of NP-GL, the TDLFP sequence was adapted as follows: IB (-25 mbar for 10 s; ~12.3 nL), NP-GL (-50 mbar for 5 s; ~12.3 nL), Myr (-50 mbar for 5 s; ~12.3 nL) and IB (-50 mbar for 10 s; ~24.6 nL). As for the off-line assays, the incubation time was optimized and a voltage of +20 kV was applied for separation in the His-AcOH buffer.

- Evaluation of V_{max} and K_m constants: For each enzymatic assay, each point was repeated (n=3). The nonlinear curve-fitting program PRISM® 5.04 (GraphPad, San Diego, California, USA) was used to evaluate V_{max} and K_m according to equation (2):

$$V_i = \frac{V_{max} \times [S]}{K_m + [S]} \qquad (2)$$

Where V_i is the reaction rate ($mM.min^{-1}$), K_m is the Michaelis–Menten constant (mM), V_{max} is the maximum reaction velocity ($mM.s^{-1}$) and [S] is the concentration (mM) of substrate (GLs).

3. Results

3.1. Analysis of GL-SH and sulfate by CE-C^4D/UV

Before conducting any enzymatic reaction, the CE analyses were optimized in order to detect simultaneously GL-SH by UV at 230 nm and sulfate small anion by C^4D. This would allow to monitor simultaneously the decrease of the GL-SH if hydrolyzed by Myr and the increase of sulfate as the product of the catalyzed reaction.

Firstly, the H_3PO_4-KH_2PO_4 buffer (pH 3, ionic strength of 40 mM) was used as BGE. In these conditions, GL-SH was detected at 1.3 min with good repeatability of migration time (RSD_{tm} = 0.45 %; n=3). The linearity was successfully assessed in the 0.02–2 mM (10-1000 ppm) concentration range with a determination coefficient (r^2) of 0.999 by plotting CPA *versus* GL-SH concentrations. In CE, any fluctuation in migration time will cause an error in peak area determination unless this latter is normalized for migration time. However, sulfate peak was not detected with the C^4D. This may be explained by the high effective mobility (μ_{eff}) of the co-ion phosphate used in the BGE (μ_{eff} ~ -25 x 10^{-5} $cm.V^{-1}.cm^{-1}$) as well as the overall high conductivity of this BGE due to the presence of K^+ cations. Indeed, it is known that the difference between the μ_{eff} of the BGE co-ion and the μ_{eff} of the analyte sulfate (μ_{eff} ~ -60 x 10^{-5} $cm.V^{-1}.cm^{-1}$) needs to be as high as possible in order to obtain high C^4D sensitivity [14,15,50]. Keeping the pH and the ionic strength constant, histidine/citric acid was used as BGE since the μ_{eff} of citrate is lower than phosphate's (-11 x 10^{-5} $cm.V^{-1}.cm^{-1}$). However, similar results were obtained. Subsequently, a BGE histidine/acetic acid with a higher pH of 4.2 (ionic strength of 40 mM) was used. The buffer capacity of this BGE is better than the one for histidine/citric acid; 58 mM *versus* 17 mM, respectively. The μ_{eff} of acetate is equal to -14 x 10^{-5}

228 $cm.V^{-1}.cm^{-1}$ which is close to the μ_{eff} of citrate. At pH 4.2, the electroosmotic flow (EOF) is more intense
229 than at pH 3.0, which decreases the apparent mobility of the anions analyzed in reverse mode *i.e.* migrating
230 in the opposite direction as EOF. In these conditions, GL-SH was successfully detected by UV at 2.4 min as
231 well as sulfate by C^4D at 0.9 min (Figure 2.a). The linearity of GL-SH peak area *versus* concentration was
232 confirmed in the 0.08–2 mM range with an excellent r^2 of 0.9999. Good repeatability was obtained for CPA
233 and t_m (RSD < 1.5 %; n=6). The calibration curve was also assessed over the wide concentration range
234 0.015–15 mM for sulfate. The r^2 value obtained was of 0.9994 confirming the linearity of the C^4D response
235 for sulfate detection. Excellent repeatability for sulfate was also obtained confirming the choice of the BGE
236 for the CE-C^4D/UV analyses.

237 **3.2 Myrosinase-mediated hydrolysis of GL-SH characterized by CE-C^4D/UV**

238 **3.2.a Linearity of GL-SH hydrolysis catalyzed by Myrosinase**

239 First, the linearity of the Myr action on the synthetized GL-SH was assessed using the pre-capillary
240 enzymatic assay presented in section 2.5 and the CE-C^4D/UV method above developed. As shown in Figure
241 2.a., a sulfate peak was detected after 10 min of incubation, at 37 °C. Moreover, Figure 2.b shows that the
242 peak area of the GL-SH quantitatively decreases while the sulfate increases over time. The enzymatic
243 reaction is linear for an incubation time of 40 min approximately. A plateau is reached after almost 60 min
244 of reaction time, which corresponds to the total consumption of the GL-SH present in the incubation
245 mixture. The results of this straightforward assay already confirm that the tested GL-SH is a substrate of the
246 myrosinase.

247 Subsequently, V_{max} and K_m parameters were determined to evaluate the affinity of this unnatural GL towards
248 the myrosinase and to compare it to sinigrin, a natural well-referenced substrate.

249 **3.2.b. Michaelis-Menten study of GL-SH hydrolysis using off-line and on-line CE-based assays**

250 The Michaelis-Menten curves of the GL-SH as well as of sinigrin were assessed using an IB at pH 7.0 which
251 corresponds to the optimum pH value for the myrosinase to be active [51]. Sinigrin was used for validation

of the developed assay and for comparison with the GL-SH in terms of affinity towards Myr. The Figure 3 shows the Michaelis-Menten curves obtained using the off-line assay for the sinigrin and the GL-SH. V_{max} and K_m values are reported in the Table 1. Results show that the unnatural GL-SH has affinity in the same range as the natural substrate sinigrin even though its structure is bulkier.

In order to decrease the consumption of substrate and enzyme from few microliters to few nanoliters, an on-line CE assay was developed for the first time to study myrosinase kinetics. This on-line assay is based on TDLFP for reactant mixing and triggering of the enzymatic reaction inside the capillary. The order of reactant plugs was based on the diffusion coefficient (D_m) of each reagent [48]. For this, the reactant injection started with the Myr (0.1 $U.mL^{-1}$) since it has the lowest D_m followed by the GL substrate (sinigrin or GL-SH) having the highest D_m. This is important to better control the incubation time of the enzymatic reaction triggered by transverse diffusion inside the capillary [48,49]. A plug of IB was injected first to prevent inactivating the enzyme by the BGE. This plug must have a rectangular shape to avoid its transversal diffusion and therefore, its injection occurred at low pressure for longer injection time than for reactant injection; -25 mbar for 10 s. A long parabolic plug of IB was also injected (-50 mbar for 10 s) at the end of the injection sequence to ensure a good mixing of the enzyme with its substrate. Taking into account the dilution occurring in the capillary after reactant mixing, the final enzyme concentration in the capillary is expected to be around 0.05 $U.mL^{-1}$, thus comparable to the one used in pre-capillary assays. However, it is well established that the dilution effect of the final IB plug is difficult to forecast [48,52].

In these conditions, a quantifiable peak of the product SO_4^{2-} was obtained after 10 min of incubation inside the capillary of sinigrin or of GL-SH with the Myr with RSD $_{CPA\ sulfate}$ inferior to 0.47 % (n = 3). Subsequently, this on-line CE assay was used to determine the V_{max} and K_m constants. Results presented in Figure 3 and Table 1 are consistent with those obtained using the off-line assay showing that the unnatural GL-SH has affinity in the same range as the natural substrate sinigrin. Moreover, it can be noticed that for both glucosinolates, the V_{max} values obtained from the on-line approach are slightly lower than the one

obtained off-line, whereas the on-line K_m values are slightly higher. This can be explained by the dilution phenomena inherent to the TDLFP method [48,52].

To conclude, V_{max} and K_m values obtained by both off-line and on-line approaches confirm that the synthetized GL-SH is a good substrate of Myr with a kinetic profile comparable to the sinigrin one. These results encouraged us to use the GL-SH to functionalize the surface of AuNPs following the schema shown in Figure 1, with the aim of setting up NPs that may easily serve as practical platforms for bioconjugaison.

3.3 Monitoring of the hydrolysis of functionalized AuNPs

3.3.a Stability of commercial AuNPs

The high surface energy of noble metal nanoparticles can induce aggregation in solution. For this, when working with AuNPs, it is essential to identify whether they are forming reversible (flocculated) or irreversible (agglomerated) clusters in solution. Haes et al. [24] introduced a CE method to evaluate the stability of the AuNPs based on the fact that if the majority of the NPs are in their isolated form in solution, they will absorb strongly at 520 nm and weakly at 600 nm (red-shifting) [24,38]. Consequently, they established that NP stability can be estimated by taking the ratio (R) of the absorbance at both wavelengths (equation 1).

In this study, the CE-UV analysis of the commercial citrate stabilized AuNPs was optimized. Indeed, it is known that despite the high degree of stability in water or buffer solution, gold citrate nanoparticles are unstable inside a capillary. The electrostatically attached citrate molecules can be lost by the influence of the electric field. Moreover, several parameters may induce uncontrolled aggregation such as temperature variations, stirring or modification of the surface chemistry as for example by adding in this study the GL-SH. For this, it was important to control the stability of the AuNPs during experimentations.

First, a background electrolyte borate (pH 9.2, I = 25 mM) was used for the analysis of these anionic NPs. The peak of NP citrates was distorted and had a low intensity. Even at higher ionic strength of 50 mM, peak

shape was still not acceptable. This may be due to the rather low stability of citrate-capped AuNPs inside the capillary [53]. Subsequently, a 10 mM CAPS containing 70 mM SDS (pH 10, I = 50 mM) was used as BGE. The presence of the surfactant SDS is expected to improve AuNP stability and to reduce uncontrolled aggregation [38]. With this BGE, a symmetrical peak was detected at 2.6 min (CPA = 62.2) by absorption at 520 nm (Figure 4.a). This peak is characteristic of isolated AuNPs. A less intense peak (CPA = 16.0) was obtained when the electropherograms were recorded at 600 nm indicating the presence of small quantities of aggregated AuNPs (Figure 4.a). Good repeatabilities (n=6) were obtained on the migration time (RSD = 0.4 %) and on the CPA (RSD = 1.7 %).

The ratio R could thus be calculated (equation 1). It was found to be 3.9 ± 0.1 (n = 3) indicating that the commercial citrate-capped AuNPs were well flocculated in solution. Indeed, R is close to 3.5-4 for flocculated nanoparticles and decreases for aggregated NPs approaching eventually 0 [24]. Since the stability of citrate AuNPs was confirmed, their functionalization by the GL-SH could be conducted.

3.3.b. Functionalization of AuNPs

Functionalization of the citrate AuNPs with GL-SH is based on a ligand exchange reaction between the external thiols of the GL-SH and the existing labile capping ligands on AuNPs *e.g.* citrates. This equilibrium process allows the synthesis of mixed monolayer-protected AuNPs. Different temperatures (4 °C, 19 °C and 25 °C) were tested (other conditions in section 2.3). The functionalized NPs, presented in this manuscript as NP-GL, were then analyzed by CE-UV using the conditions optimized in the previous section 3.3.a.

When the functionalization was carried out at low temperature 4 °C, the electropherograms were similar to those plotted for the analysis of commercial citrate AuNPs with a peak detected at 2.6 min. A peak at 2.9 min (Figure 4.b) was obtained when working at higher temperature. Moreover, excellent repeatabilities (n = 6) on migration time (RSD = 0.3 %) and on CPA (RSD = 1.2 %) were obtained when conducting the functionalization at 25 °C. The shift in the migration time *i.e.* in the electrophoretic mobility of these anions

323 - since the electroosmotic flow is constant - indicates a modification of the surface of the AuNPs. This is
324 certainly due to the citrate on the AuNPs being displaced by the GL-SH.
325 Figure 4.b also shows that the GL-SH free in solution can be detected at 230 nm with a longer migration
326 time equal to 3.6 min. GL-SH migrates as an anion, like the citrate AuNPs and the NP-GL.
327 It is essential to note that, no free GL-SH was detected when analyzing the NP-GL, which confirms the
328 efficiency of the centrifugation/washing steps of the NPs. Moreover, the ratio R was also calculated for the
329 functionalized AuNPs. The value obtained was 3.8 ± 0.1 (n=6) indicating that the NP-GL were still
330 flocculated in solution. The hydrolysis of these glucosinolate functionalized nanoparticles was therefore
331 studied using the CE-C^4D/UV approach developed in section 3.1.
332 **3.3.c. Myrosinase-mediated hydrolysis of NP-GL characterized by CE-C^4D/UV**
333 First, the on-line assay was conducted due to the interesting economy of this approach. The NP-GL were
334 injected before Myr since they have a lower D_m (other conditions in section 2.5). The sulfate was
335 successfully detected at 0.9 min with a CPA increasing with the incubation time (5, 10 and 20 min). On the
336 other hand, no free GL-SH was detected simultaneously using UV detection. This is a very interesting result
337 showing that: (i) the sulfate detected is produced by the action of the Myr exclusively on the GL-SH
338 immobilized on the AuNPs; and (ii) the Myr is still able to catalyze the hydrolysis of the GL-SH even when
339 immobilized on the AuNPs. Moreover, this also demonstrates that TDLFP can be used for mixing nano-
340 material with the protein Myr of much smaller size. However, this mixing process is limited by the
341 sedimentation of the NPs inside the capillary. Indeed, when the incubation time is relatively high, higher
342 than 20 min, the reaction was limited resulting in a relatively small increase of the sulfate peak.
343 Consequently, the pre-capillary approach was then evaluated. As for on-line assay, the sulfate was
344 successfully detected by the C^4D at 0.9 min with good repeatability (RSD = 0.39 %; n = 3) and no free GL-
345 SH was detected by UV. The advantage of this approach over the on-line assay is that the incubation time
346 could be increased to several hours. The CPA of the product SO_4^{2-} detected by the C^4D for the hydrolysis of

two batches of NP-GL prepared freshly or after one week of conservation at 4°C were plotted as a function of the incubation time (Figure 5). The interval of time was equal to 10 min and the functionalization of the NPs was conducted at 25 °C. This time-dependent following of the enzyme reaction (continuous assay) is important for evaluating the myrosinase activity towards its substrate, the NP-GL in this case. CE results show that NP-GL are stable at 4°C for at least one week and that the batch-to-batch reproducibility is acceptable. Indeed, it can be seen that all the three curves in Figure 5 present the same trend, corresponding to the progress curve of a typical enzyme reaction. The sulfate quantity increases in a linear manner for an incubation time less than 40 min ($r^2 > 0.985$) which compares well with the linearity obtained for the hydrolysis of the free GL-SH (Figure 2.b). However, the plateau is reached for GL-SH immobilized on the AuNP after almost 150 min of incubation (Figure 5) whereas it was reached after 60 min for the free GL-SH (Figure 2.b). The slower kinetics observed can be explained by diffusion limitations due to reactant immobilization [54,55]. On the other hand, it is worthy to note that when conducting NP-GL functionalization at 19 °C, the quantities of SO_4^{2-} released were lower than those obtained with NP-GL at 25°C. The grafting of AuNPs at 25 °C is thus more efficient.

4. Conclusion

In this work, CE with dual detection C^4D/UV was introduced as an all-in-one tool for monitoring an original process of functionalization of gold nanoparticles based on the myrosinase-glucosinolate reaction. First, a CE method was developed to simultaneously detect by UV any decrease of the GL-SH substrate when hydrolyzed by Myr, and by C^4D any increase of sulfate as the product of the catalyzed reaction. The linearity of GL-SH and sulfate peak area *versus* concentration was confirmed with an excellent r^2 higher than 0.999. Good repeatabilities were also obtained confirming that the electrophoretic conditions chosen were adapted for the dual detection system, C^4D and UV. Offline and online CE-assays both confirmed that the synthesized GL-SH is a good substrate of Myr with a kinetic profile comparable to the sinigrin one. In

addition, CE was established as a tool to follow-up and to confirm the stability of citrate AuNPs before and after the functionalization of their surface by GL-SH. The hydrolysis of glucosinolate functionalized nanoparticles was subsequently studied using the developed CE-C^4D/UV approach. It was demonstrated that Myr was able to hydrolyze the functionalized nanoparticles. The rapidity and the economy of this technique allowed to follow this entire process using low reaction volumes and with only few minutes of analysis time. Moreover, it was possible to confirm the compatibility of the myrosinase-glucosinolate system with the on-line CE based assays with an important advantage in term of reagent consumption.

This work opens the way to further promising investigations concerning the use of CE to follow the functionalization of AuNPs using the enzymatically produced isothiocyanate function as a reactive moiety to anchor biologically relevant biomolecules.

Declaration of interests

The authors declare that they have no known competing financial interests or personal relationships that could have appeared to influence the work reported in this paper.

The authors declare the following financial interests/personal relationships, which may be considered as potential competing interests.

Acknowledgements: This work has been supported by the University of Orleans (France), the CNRS (Centre National de la Recherche Scientifique, France) and the Labex SynOrg (ANR-11-LABX-0029).

391 **Figure list**

392 **Figure 1.** Mechanism of gold-nanoparticles functionalization by GL-SH (1st step) and their hydrolysis to
393 obtain isothiocyanate valuable for bio-conjugation (2nd step).

394 **Figure 2**. Myrosinase-mediated hydrolysis of GL-SH monitored by CE-C^4D/UV. **a**) Example of
395 electropherograms; **b)** Linearity study of the enzymatic reaction.

396 Experimental conditions: Reaction mixture (11 µL total volume): incubation buffer KH_2PO_4/K_2HPO_4 (pH
397 7.0, ionic strength 33 mM); myrosinase (0.05 $U.mL^{-1}$); GL-SH (1.6 mM). Incubation at 37 °C for 10 min.
398 Capillary *electrophoresis*: silica capillary: 31 cm x 8.5 cm x 50 µm i.d. (short-end injection); BGE:
399 histidine/acetic acid buffer (pH 4.4, ionic strength 40 mM). Electrophoretic separation: +20 kV at 25 °C
400 (current 31 µA). Short-end injection: -50 mbar × 10 sec (24.6 nL). Rinse between analyses: 3 min BGE. C^4D
401 detector: frequency medium, voltage 0 dB, gain 100 %, offset 130, filter: frequency 1/3 and cut-off 0.05. UV
402 detection of GL-SH was conducted at 230 nm.

403 **Figure 3. a)** Michaelis-Menten plots for myrosinase-mediated hydrolysis of **a)** sinigrin and **b)** GL-SH
404 obtained by off-line and on-line assays.

405 For experimental conditions: see figure 2 and section 2.5.

406 **Figure 4.** Electropherograms obtained **a)** for commercial NP citrates at 520 nm and 600 nm, and **b)** for NP
407 citrates (520 nm), NP-GL (520 nm) and free GL-SH (230 nm).

408 Experimental conditions: silica capillary: 40 cm x 31.5 cm x 50 µm i.d.. BGE: 10 mM CAPS-70 mM SDS
409 buffer (pH 10). Electrophoretic separation: +20 kV at 25 °C (current 61 µA). Normal injection: 50 mbar × 30
410 sec (57 nL). Rinse between analyses: 3 min BGE.

411 **Figure 5.** Myrosinase-mediated hydrolysis of NP-GL characterized by CE-C^4D/UV using off-line CE-based
412 enzymatic assays.

413 Reproducibility between batches was evaluated as well as the stability of the functionalized gold NP.
414 Experimental conditions: Fig. 2.

References

[1] S. Gattu, C.L. Crihfield, G. Lu, L. Bwanali, L.M. Veltri, L.A. Holland, Advances in enzyme substrate analysis with capillary electrophoresis, Methods 146 (2018) 93-106.

[2] M. Cheng, Z. Chen, Recent advances in screening of enzymes inhibitors based on capillary electrophoresis, J. Pharm. Anal. 8 (2018) 226-233.

[3] S. Huang, P. Paul, P. Ramana, E. Adams, P. Augustijns, A. Van Schepdael, Advances in capillary electrophoretically mediated microanalysis for on-line enzymatic and derivatization reactions, Electrophoresis 39 (2018) 97-110.

[4] S. Fayad, P. Morin, R. Nehmé, Use of chromatographic and electrophoretic tools for assaying elastase, collagenase, hyaluronidase, and tyrosinase activity, J. Chromatogr. A 1529 (2017) 1-28.

[5] R. Nehmé, P. Morin, Advances in capillary electrophoresis for miniaturizing assays on kinase enzymes for drug discovery, Electrophoresis 36 (2015) 2768-2797.

[6] J. Bao, F.E. Regnier, Ultramicro enzyme assays in a capillary electrophoretic system, Journal of Chromatography A 608 (1992) 217-224.

[7] B.J. Harmon, I. Leesong, F.E. Regnier, Moving boundary electrophoretically mediated microanalysis, J. Chromatogr. A 726 (1996) 193-204.

[8] S. Van Dyck, A. Van Schepdael, J. Hoogmartens, Michaelis-Menten analysis of bovine plasma amine oxidase by capillary electrophoresis using electrophoretically mediated microanalysis in a partially filled capillary, Electrophoresis 22 (2001) 1436-1442.

[9] V. Okhonin, X. Liu, S.N. Krylov, Transverse diffusion of laminar flow profiles to produce capillary nanoreactors, Anal. Chem. 77 (2005) 5925-5929.

[10] H. Nehmé, R. Nehmé, P. Lafite, S. Routier, P. Morin, New development in in-capillary electrophoresis techniques for kinetic and inhibition study of enzymes, Anal. Chim. Acta 722 (2012) 127-135.

[11] H. Nehmé, R. Nehmé, P. Lafite, E. Duverger, S. Routier, P. Morin, Electrophoretically mediated microanalysis for in-capillary electrical cell lysis and fast enzyme quantification by capillary electrophoresis, Anal. Bioanal. Chem. 405 (2013) 9159-9167.

[12] J. Iqbal, S. Iqbal, C.E. Müller, Advances in immobilized enzyme microbioreactors in capillary electrophoresis, Analyst 138 (2013) 3104-3116.

[13] J. Ferey, D. Da Silva, C. Colas, R. Nehmé, P. Lafite, V. Roy, P. Morin, R. Daniellou, L. Agrofoglio, B. Maunit, Monitoring of successive phosphorylations of thymidine using free and immobilized human nucleoside/nucleotide kinases by Flow Injection Analysis with High-Resolution Mass Spectrometry, Anal. Chim. Acta 1049 (2019) 115-122.

[14] A.J. Zemann, E. Schnell, D. Volgger, G.K. Bonn, Contactless conductivity detection for capillary electrophoresis, Anal. Chem. 70 (1998) 563-567.

[15] J.A. Fracassi da Silva, C.L. do Lago, An oscillometric detector for capillary electrophoresis, Anal. Chem. 70 (1998) 4339-4343.

[16] S. Fayad, M. Tannoury, P. Morin, R. Nehmé, Simultaneous elastase-, hyaluronidase- and collagenase-capillary electrophoresis based assay. Application to evaluate the bioactivity of the red alga *Jania rubens*, Anal. Chim. Acta 1020 (2018) 134-141.

[17] S. Fayad, R. Nehmé, M. Langmajerová, B. Ayela, C. Colas, B. Maunit, J.-C. Jacquinet, A. Vibert, C. Lopin-Bon, Z. Glatz, P. Morin, Hyaluronidase reaction kinetics evaluated by capillary electrophoresis with UV and high-resolution mass spectrometry (HRMS) detection, Anal. Chim. Acta 951 (2017) 140-150.

[18] Y. Ladner, S. Mas, G. Coussot, K. Bartley, J. Montels, J. Morel, C. Perrin, Integrated microreactor for enzymatic reaction automation: An easy step toward the quality control of monoclonal antibodies, Journal of Chromatography A 1528 (2017) 83-90.

[19] K.D. Greis, Mass spectrometry for enzyme assays and inhibitor screening: an emerging application in pharmaceutical research, Mass Spec. Rev. 26 (2007) 324-339.

[20] M. Moini, Capillary electrophoresis mass spectrometry and its application to the analysis of biological mixtures, Anal. Bioanal. Chem. 373 (2002) 466-480.

[21] L. Licklider, W.G. Kuhr, M.P. Lacey, T. Keough, M.P. Purdon, R. Takigiku, Online microreactors/capillary electrophoresis/mass spectrometry for the analysis of proteins and peptides, Anal. Chem. 67 (1995) 4170-4177.
[22] A.A. Elbashir, O.J. Schmitz, H.Y. Aboul-Enein, Application of capillary electrophoresis with capacitively coupled contactless conductivity detection (CE-C4D): An update, Biomed. Chromatogr. 31 (2017) e3945.
[23] C. Haber, R.J. Van Saun, W.R. Jones, Quantitative analysis of anions at ppb/ppt levels with capillary electrophoresis and conductivity detection: enhancement of system linearity and precision using an internal standard, Anal. Chem. 70 (1998) 2261-2267.
[24] M.R. Ivanov, H.R. Bednar, A.J. Haes, Investigations of the mechanism of gold nanoparticle stability and surface functionalization in capillary electrophoresis, ACS Nano. 3 (2009) 386-394.
[25] Á.I. López-Lorente, M.L. Soriano, M. Valcárcel, Analysis of citrate-capped gold and silver nanoparticles by thiol ligand exchange capillary electrophoresis, Microchim. Acta 181 (2014) 1789-1796.
[26] E. Ban, Y.S. Yoo, E.J. Song, Analysis and applications of nanoparticles in capillary electrophoresis, Talanta 141 (2015) 15-20.
[27] A. Pallotta, A. Boudier, P. Leroy, I. Clarot, Characterization and stability of gold nanoparticles depending on their surface chemistry: Contribution of capillary zone electrophoresis to a quality control, J. Chromatogr. A 1461 (2016) 179-184.
[28] G.R. Sarria, M.Á. Berenguer Francés, I. Linares Galiana, Enhancing radiotherapy effect in breast cancer with nanoparticles: A review, Rep. Pract. Oncol. Radiother. 24 (2019) 65-67.
[29] F. Fathi, M.-R. Rashidi, Y. Omidi, Ultra-sensitive detection by metal nanoparticles-mediated enhanced SPR biosensors, Talanta 192 (2019) 118-127.
[30] H. Agarwal, A. Nakara, V.K. Shanmugam, Anti-inflammatory mechanism of various metal and metal oxide nanoparticles synthesized using plant extracts: A review, Biomed. Pharmacother. 109 (2019) 2561-2572.
[31] X.-M. Ma, M. Sun, Y. Lin, Y.-J. Liu, F. Luo, L.-H. Guo, B. Qiu, Z.-Y. Lin, G.-N. Chen, Review: Progress of visual biosensor based on gold nanoparticles, Chinese J. Anal. Chem. 46 (2018) 1-10.
[32] Kapur M., Soni K., K. Kohli, Green synthesis of selenium nanoparticles from broccoli, characterization, application and toxicity, Adv. Tech. Biol. Med. 5 (2017) 198-204.
[33] H. Jans, X. Liu, L. Austin, G. Maes, Q. Huo, Dynamic light scattering as a powerful tool for gold nanoparticle bioconjugation and biomolecular binding studies, Anal. Chem. 81 (2009) 9425-9432.
[34] T. Muangnapoh, N. Sano, S.-I. Yusa, N. Viriya-empikul, T. Charinpanitkul, Facile strategy for stability control of gold nanoparticles synthesized by aqueous reduction method, Curr. Appl. Phys. 10 (2010) 708-714.
[35] X. Qian, X.-H. Peng, D.O. Ansari, Q. Yin-Goen, G.Z. Chen, D.M. Shin, L. Yang, A.N. Young, M.D. Wang, S. Nie, *In vivo* tumor targeting and spectroscopic detection with surface-enhanced Raman nanoparticle tags, Nat. Biotechnol. 26 (2007) 83-90.
[36] F.-K. Liu, Analysis and applications of nanoparticles in the separation sciences: A case of gold nanoparticles, J. Chromatogr. A 1216 (2009) 9034-9047.
[37] N. Wangoo, K.K. Bhasin, R. Boro, C.R. Suri, Facile synthesis and functionalization of water-soluble gold nanoparticles for a bioprobe, Anal. Chim. Acta 610 (2008) 142-148.
[38] Y.-C. Yeh, B. Creran, V.M. Rotello, Gold nanoparticles: preparation, properties, and applications in bionanotechnology, Nanoscale 4 (2012) 1871-1880.
[39] M. Zarei, M. Zarei, M. Ghasemabadi, Nanoparticle improved separations: From capillary to slab gel electrophoresis, Trends Anal. Chem. 86 (2017) 56-74.
[40] A. Pallotta, M. Parent, I. Clarot, M. Luo, V. Borr, P. Dan, V. Decot, P. Menu, R. Safar, O. Joubert, P. Leroy, A. Boudier, Blood compatibility of multilayered polyelectrolyte films containing immobilized gold nanoparticles, Part. Part. Syst. Char. 34 (2017) (1-8) 1600184.
[41] M. Khoobchandani, A. Zambre, K. Katti, C.-H. Lin, K.V. Katti, Green nanotechnology from *Brassicaceae*: development of broccoli phytochemicals–encapsulated gold nanoparticles and their applications in nanomedicine, Int. J. Green Nanotechnol. 1 (2013) 1-15.

[42] P. Kuppusamy, S.J.A. Ichwan, N.R. Parine, M.M. Yusoff, G.P. Maniam, N. Govindan, Intracellular biosynthesis of Au and Ag nanoparticles using ethanolic extract of Brassica oleracea L. and studies on their physicochemical and biological properties, J. Environ. Sci. 29 (2015) 151-157.
[43] V. Gil, A.J. MacLeod, Studies on glucosinolate degradation in *Lepidium sativum* seed extracts, Phytochem. 19 (1980) 1369–1374.
[44] A. Bourderioux, M. Lefoix, D. Gueyrard, A. Tatibouët, S. Cottaz, S. Arzt, W.P. Burmeister, P. Rollin, The glucosinolate–myrosinase system. New insights into enzyme–substrate interactions by use of simplified inhibitors, Org. Biomol. Chem. 3 (2005) 1872-1879.
[45] G. Cutolo, F. Reise, M. Schuler, R. Nehmé, G. Despras, J. Brekalo, P. Morin, P.Y. Renard, T.K. Lindhorst, A. Tatibouët, Bifunctional mannoside–glucosinolate glycoconjugates as enzymatically triggered isothiocyanates and FimH ligands, Org. Biomol. Chem. 16 (2018) 4900-4913.
[46] J.W. Fredy, G. Cutolo, B. Poret, R. Nehmé, M. Hubert-Roux, P. Gandolfo, H. Castel, M. Schuler, A. Tatibouët, C. Sabot, P.-Y. Renard, Diverted natural Lossen-type rearrangement for bioconjugation through *in situ* myrosinase-triggered isothiocyanate synthesis, Bioconjugate Chem. 30 (2019) 1385-1394.
[47] R. Nehmé, H. Nehmé, G. Roux, D. Cerniauskaite, P. Morin, P. Rollin, A. Tatibouët, Contactless conductivity detection for screening myrosinase substrates by capillary electrophoresis, Anal. Chim. Acta 807 (2014) 153–158.
[48] S.M. Krylova, V. Okhonin, S.N. Krylov, Transverse diffusion of laminar flow profiles - a generic method for mixing reactants in capillary microreactor, J. Sep. Sci. 32 (2009) 742-756.
[49] H. Nehmé, R. Nehmé, P. Lafite, S. Routier, P. Morin, Human protein kinase inhibitor sceening by capillary electrophoresis using transverse diffusion of laminar flow profiles for reactant mixing, J. Chromatogr. A 1314 (2013) 298-305.
[50] R. Nehmé, A. Lascaux, R. Delépée, B. Claude, P. Morin, Capillary electrophoresis procedure for the simultaneous analysis and stoichiometry determination of a drug and its counter-ion by using dual-opposite end injection and contactless conductivity detection: Application to labetalol hydrochloride, Anal. Chim. Acta 663 (2010) 190-197.
[51] S. Palmieri, O. Leoni, R. Iori, A steady-state kinetics study of myrosinase with direct ultraviolet spectrophotometric assay, Anal. Biochem. 123 (1982) 320-324.
[52] R. Nehmé, H. Nehmé, T. Saurat, M.-L. de-Tauzia, F. Buron, P. Lafite, P. Verrelle, E. Chautard, P. Morin, S. Routier, H. Bénédetti, New in-capillary electrophoretic kinase assays to evaluate inhibitors of the PI3k/Akt/mTOR signaling pathway, Anal. Bioanal. Chem. 406 (2014) 3743-3754.
[53] B. Neiman, E. Grushka, O. Lev, Use of gold nanoparticles to enhance capillary electrophoresis, Anal. Chem. 73 (2001) 5220-5227.
[54] B.K. Hamilton, C.R. Gardner, C.K. Colton, Effect of diffusional limitations on lineweaver-burk plots for immobilized enzymes, AIChE J. 20 (1974) 503-510.
[55] J. Schejbal, S. Sefrana, R. Reminek, Z. Glatz, Capillary electrophoresis integrated immobilized enzyme reactor for kinetic and inhibition assays of beta-secretase as the Alzheimer's disease drug target, J. Sep. Sci. 42 (2019) 1067-1076.

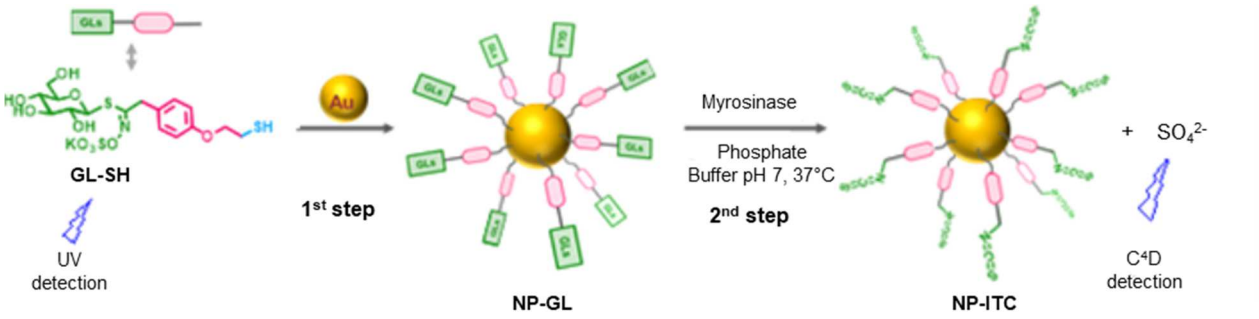
GL-SH
UV
detection
Au
1st step
NP-GL
Myrosinase
Phosphate
Buffer pH 7, 37°C
2nd step
NP-ITC
+ SO4 2-
C4D
detection

Figure 1

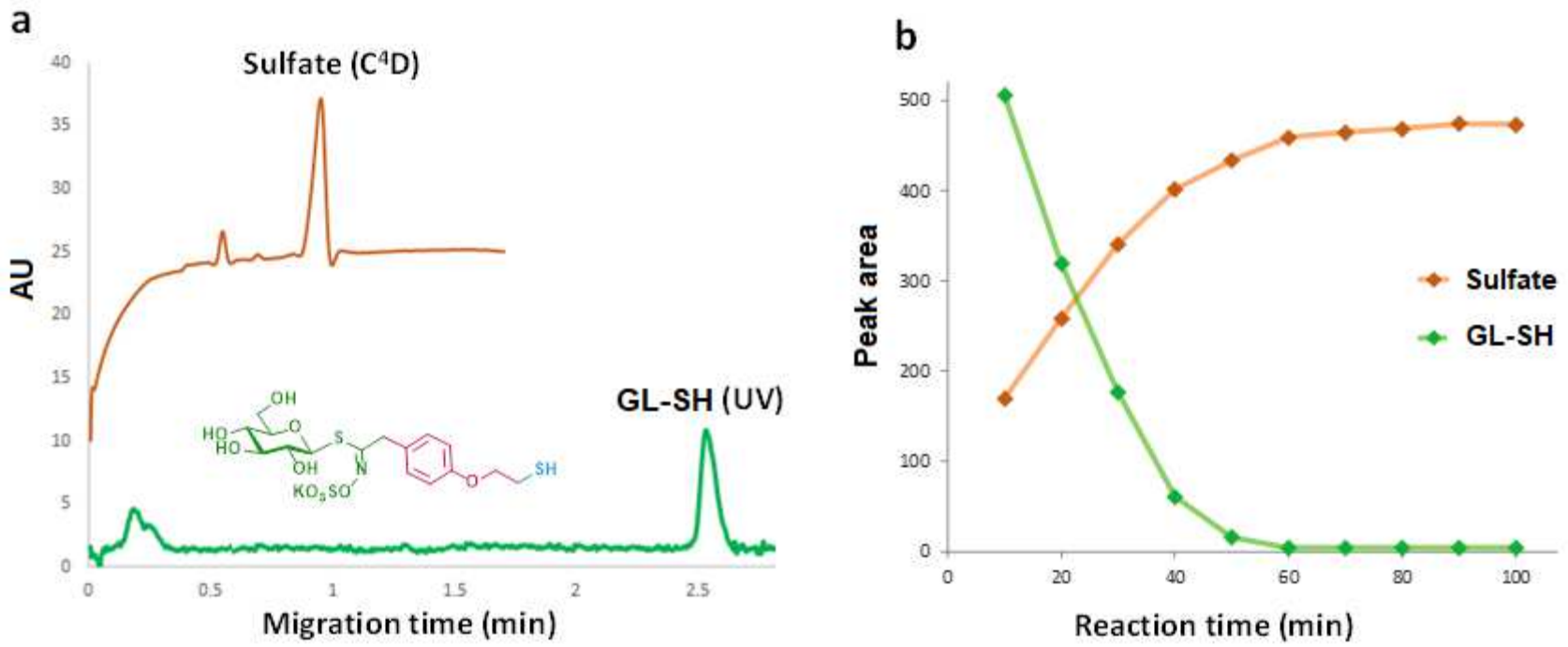
a
Sulfate (C4D)
GL-SH (UV)
AU
Migration time (min)
b
Peak area
Reaction time (min)
Sulfate
GL-SH

Figure 2

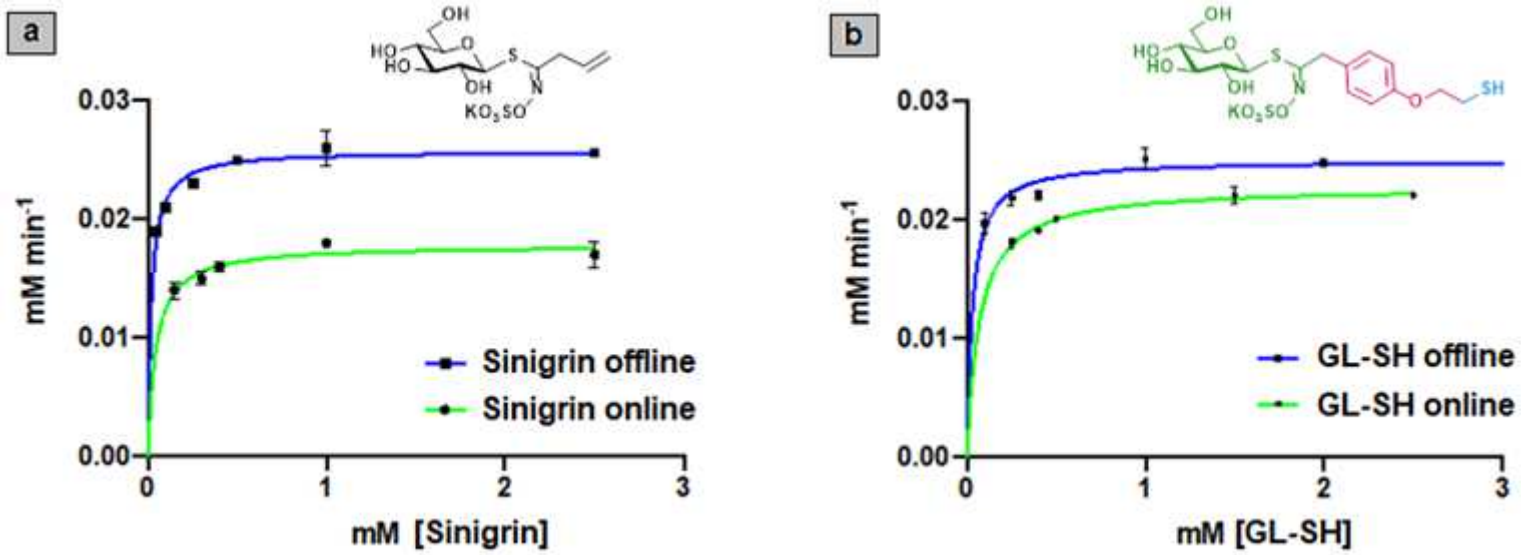
a
b
mM min-1
0.03
0.02
0.01
0.00
0
1
2
3
mM [Sinigrin]
Sinigrin offline
Sinigrin online
mM [GL-SH]
GL-SH offline
GL-SH online
OH
HO
O
S
N
KO3SO
SH

Figure 3

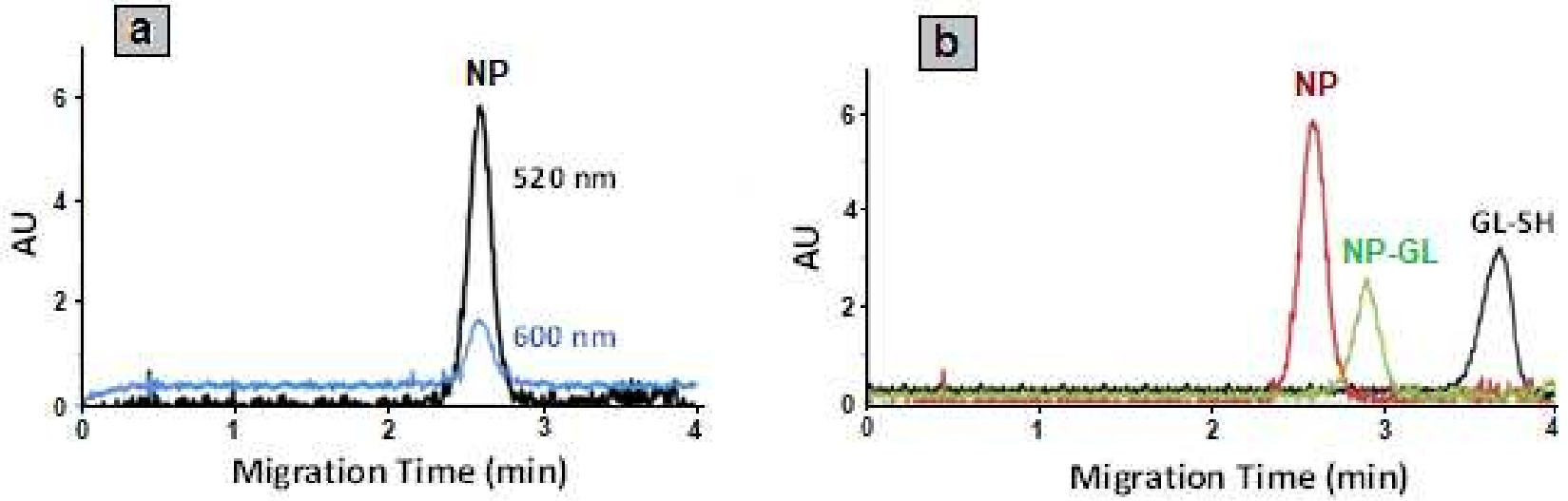
a
NP
520 nm
600 nm
AU
Migration Time (min)
b
NP
NP-GL
GL-SH
AU
Migration Time (min)

Figure 4

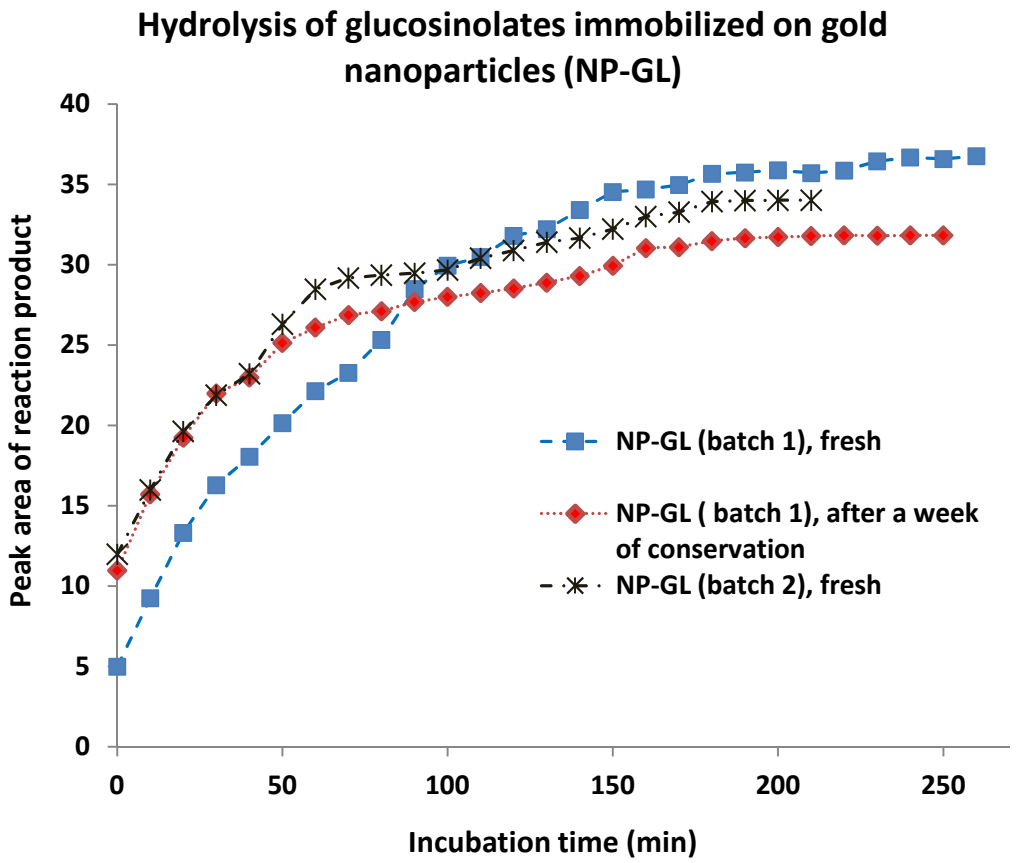
Hydrolysis of glucosinolates immobilized on gold nanoparticles (NP-GL)
Peak area of reaction product
Incubation time (min)
0
5
10
15
20
25
30
35
40
0
50
100
150
200
250
NP-GL (batch 1), fresh
NP-GL (batch 1), after a week of conservation
NP-GL (batch 2), fresh

Figure 5

Table 1 : K_m and V_{max} for sinigrin and GL-SH using off-line and on-line CE-C^4D/UV assay

	Off-line		On-line	
	V_{max} (µM min^{-1})	K_m (µM)	V_{max} (µM min^{-1})	K_m (µM)
Sinigrin	25.8 ± 2.1	20.0 ± 2.6	17.8 ± 0.9	44.1 ± 3.9
GL-SH	24.9 ± 1.3	30.6 ± 3.6	22.7 ± 1.7	69.7 ± 4.1

Hydrolysis of glucosinolates immobilized on gold nanoparticles (NP-GL)